Solar RRL
www.solar-rrl.com

Dangling Bond Defects on Si Surfaces and Their Consequences on Energy Band Diagrams: From a Photoelectrochemical Perspective

Dominik C. Moritz, Wolfram Calvet, Mohammad Amin Zare Pour, Agnieszka Paszuk, Thomas Mayer, Thomas Hannappel, Jan P. Hofmann, and Wolfram Jaegermann**

Using silicon in multijunction photocells leads to promising device structures for direct photoelectrochemical water splitting. In this regard, photoelectron spectra of silicon surfaces are used to investigate the energetic condition of contact formation. It is shown that the Fermi-level position at the surface differs from the values expected from their bulk doping concentrations, indicating significant surface band bending which may limit the overall device efficiency. In this study, the influence of different surface preparation procedures for p- and n-doped Si wafers on surface band bending is investigated. With the help of photoemission and X-ray absorption spectroscopy, Si dangling bonds are identified as dominating defect centers at Si surfaces. These defects lead to an occupied defect band in the lower half and an unoccupied defect band in the upper half of the Si bandgap. However, partial oxidation of the defect centers causes a shift of defect bands, with only donor states remaining in the Si bandgap. Source-induced photovoltages at cryogenic temperatures indicate that partial surface oxidation also decreases the recombination activity of these defect centers. It is shown that defect distribution, defect concentration, and source-induced photovoltages need to be considered when analyzing Fermi-level pinning at Si surfaces.

1. Introduction

Photoelectrochemical water splitting allows direct conversion and storage of solar energy by molecular hydrogen formation. In the past decades, photoelectrochemical water splitting using III–V group multijunction devices could reach solar-to-hydrogen efficiencies of more than 19%.[1] Using thin-film triple cells from amorphous and polycrystalline Si, which may be considered as a large-scale and cheap alternative, a conversion efficiency of nearly 10% has been reached.[2] However, a fundamental understanding of the electronic structure and energetic band alignment at the solid–electrolyte interface with respect to relative energetic positions as well as the formation of electronic surface states is missing in order to bring the overall device efficiency to its physical limits.[3] Photoelectrodes of crystalline and amorphous silicon provide interesting device structures when combined to multijunction cells[2,4] and nanorod structures.[5] In addition, Si-based photoelectrodes provide valuable reference systems due to their large numbers of fundamental and application-related investigations manifested in the literature. Although surface preparation of Si has been investigated for many decades and wet chemical surface preparation for native oxide etching as well as electronic surface passivation became a widely and common method in Si wafer processing,[6–8] the role of surface defects with respect to photoelectrochemical applications is not fully understood yet.[9,10] The chemically harsh conditions at photoelectrochemical interfaces require a deeper understanding of the energetic role of surface defects, with respect to chemical environment and electronic distribution of the defect centers in order to identify Fermi-level pinning mechanisms leading to barrier formation and trapping of excess charge carriers.[10,11] Due to the lack of bonding partners in 1D, nonsaturated bonding states, that is, dangling bonds, appear at the Si surface and thus form the dominating surface defect. The paramagnetic and diamagnetic character of such trivalent $Si_3 \equiv Si\cdot$ dangling bonds, depending on the electronic occupation of the defect, has been identified as so-called P_b centers at the interface to a native oxide layer and are well studied with electron paramagnetic resonance (ESR) as well as spin-dependent recombination (SDR).[12,13] The formation of Si–O-, Si–H-, or Si–R-terminated surfaces leads in case of perfect adsorbate covered dangling bond states to an electronic and chemical passivation of the Si surfaces. The quality of these passivation layers corresponds to the number of remaining dangling bonds and depends on surface orientation

D. C. Moritz, W. Calvet, T. Mayer, J. P. Hofmann, W. Jaegermann
Department of Materials and Earth Sciences
Surface Science Laboratory
Technical University of Darmstadt
Otto-Berndt-Straße 3, 64287 Darmstadt, Germany
E-mail: dmoritz@surface.tu-darmstadt.de; jaegermann@surface.tu-darmstadt.de

M. A. Zare Pour, A. Paszuk, T. Hannappel
Institute of Physics
Fundamentals of Energy Materials
Ilmenau University of Technology
Gustav-Kirchhoff-Straße 5, 98693 Ilmenau, Germany

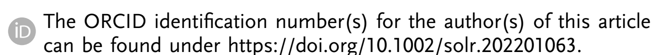
The ORCID identification number(s) for the author(s) of this article can be found under https://doi.org/10.1002/solr.202201063.

© 2023 The Authors. Solar RRL published by Wiley-VCH GmbH. This is an open access article under the terms of the Creative Commons Attribution License, which permits use, distribution and reproduction in any medium, provided the original work is properly cited.

DOI: 10.1002/solr.202201063

and quality of the surface passivation treatment.[7,11] However, to our knowledge, occupied and unoccupied dangling bond states inside the Si bandgap have not been investigated yet using photoemission spectroscopy (PES) and X-ray absorption spectroscopy (XAS), respectively. PES experiments allow to link the observed defect states with surface band bending and thus enable us to draw conclusions about the impact of surface preparation on Fermi-level pinning. Furthermore, our XPS measurements at liquid nitrogen temperature give detailed information on surface photovoltages (SPV) in order to examine the recombination activity of observed defects on the investigated Si surfaces.

2. Experimental Section

2.1. Preparation of Silicon Surfaces

If not otherwise stated, samples were prepared and analyzed in the Darmstadt's Integrated System for FUNdamental research (DAISY-FUN). The silicon single crystals were supplied as $10 \times 10\,\text{mm}^2$ cut wafers by Silchem Handelgesellschaft mbH, CrysTec GmbH, and Si-Mat -Silicon Materials e.K., with electronic bulk specifications determined by Hall measurements (**Table 1**). Wafers that were not wet chemically treated were rinsed with acetone and isopropyl alcohol subsequently for 10 min in an ultrasonic bath before being loaded to the ultra-high vacuum (UHV) system.

2.1.1. Flash Annealing Treatment

The flashed samples were obtained from (100)-oriented wafers which were flash annealed by a direct electron beam impact (1 kV acceleration voltage) onto the sample back side for about 3 s to up to 1400 °C (sample name: flash). The well-defined 2×1 reconstruction monitored by LEED was achieved by subsequent UHV annealing at 300 °C for 3 h (flash-2×1) under base pressures at room temperature of $< 10^{-9}$ mbar.

2.1.2. Oxygen Termination

The native oxide (nat. Ox) was analyzed as received from the supplier. Prior to preparation of a thermal oxide (therm. Ox) layer, the wafer was smoothly radio frequency sputtered for 5 min (5 W at 0.5 Pa Ar). Subsequently, it was annealed for 5 h in 0.5 Pa O_2 atmosphere at 275 °C. Oxide thicknesses d_{SiO_2} were obtained from XPS intensities of bulk I_{Si} and oxide I_{SiO_2} taking raw areas of Shirley background-subtracted Si 2p spectra according to Equation (1) using the inelastic mean free path $\lambda_{SiO_2}(E_{kin} = 1400\,\text{eV}) = 3.8\,\text{nm}$[14] and $R_0 = 0.88$.[15]

$$d_{SiO_2} = \lambda_{SiO_2} \cdot \ln\left(1 + \frac{I_{SiO_2}/I_{Si}}{R_0}\right) \tag{1}$$

Oxide stoichiometry was calculated using atomic sensitivity factors[16] and thin film-related escape depth corrections as explained in the supporting information. For these oxide-covered samples, no LEED images could be obtained, as expected.

2.1.3. Hydrogen Termination

The dry-H-terminated samples (dry-H) were prepared by annealing in H_2 atmosphere in a commercial Aixtron metal–organic chemical vapor deposition (MOCVD, AIX200) reactor. p- and n-Si(100) substrates with 2° offcut toward [110] direction were used. A wet chemical pretreatment was applied to the Si(100) substrates before processing in the MOCVD reactor. The pretreatment consisted of 1) boiling the substrates in a 1:1:6 mixture of ammonium hydroxide (NH_4OH, 25%), hydrogen peroxide (H_2O_2, 30%), and deionized (DI) water (H_2O) to remove organic contamination and metals (RCA1); 2) dipping Si(100) for 10 s in

Table 1. List of prepared samples with specifications and short description.

Index	Name	Wafer/orientation	Surface treatment/termination	LEED reconstruction†	BE/eV Si $2p_{3/2}$
i_a	flash	p-(100)	Flashed surface/deoxidized	None	99.33
i_b	flash	n-(100)	Flashed surface/deoxidized	None	99.56
ii_a	flash-2×1	p-(100)	Annealed after flashing	2×1	99.46
iii_a	nat. Ox	p-(100)	Native oxide (no further treatment)	None	99.48
iii_b	nat. Ox	n-(100)	Native oxide (no further treatment)	None	99.74
iv_a	therm. Ox	p-(100)	Sputter-annealed oxide	None	99.25
iv_b	therm. Ox	n-(100)	Sputter-annealed oxide	None	99.59
v_a	dry-H	p-(100)$^{a)}$	H_2-annealed H-terminated surface	2×2	99.23
v_b	dry-H	n-(100)$^{a)}$	H_2-annealed H-terminated surface	1×1	99.68
vi_a	111-H	p-(111)	Wet chemical H terminated	–	99.35
vi_b	111-H	n-(111)	Wet chemical H terminated	1×1	99.88
vi_c	111-H	p-(111)	H terminated stored for 4 weeks in UHV	–	99.40
vii_a	100-H	p-(100)	Wet chemical H terminated	–	99.34
vii_b	100-H	n-(100)	Wet chemical H terminated	1×1	99.81

a)Wafer with divergent doping concentrations † are shown in supplementary information.

© 2023 The Authors. Solar RRL published by Wiley-VCH GmbH

HF (10%) diluted in water (1:4); and 3) thin oxide layer formation (RCA2). The Si(100) substrates were annealed at 1000 °C for 30 min at 950 mbar H_2 pressure in order to remove the oxide layer.[17] Subsequently, the Si(100) substrates were cooled to 740 °C to prepare a H-terminated, double-layer stepped surface with prevalence of (2 × 1) domains.[18,19] This step was controlled in situ by reflection anisotropy spectroscopy (RAS, Laytec EpiRAS 200).[20] Samples were contamination free transferred from the MOCVD reactor at Technical University of Ilmenau via a dedicated ultrahigh-vacuum transfer shuttle[21] with base pressures $< 5 \times 10^{-10}$ mbar to Technical University of Darmstadt and finally loaded to DAISY-FUN without breaking vacuum.

The wet chemical hydrogen termination was prepared according to Angermann et al.[7] by etching the oxide of the (100) (100–H) and (111) (111–H) wafers for 10 min at 80 °C in piranha solution $(1{\cdot}H_2SO_4(96\%) : 1{\cdot}H_2O_2)$ and 6.5 min at room temperature in buffered 5% hydrofluoric acid $(1{\cdot}HF(40\%) : 7{\cdot}NH_4F(40\%))$. Subsequently, the etching step in piranha solution was repeated and finally the samples were etched in ammonium fluoride $(NH_4F, 40\%)$ for 10 min. The samples were rinsed after every etching step with DI water. After preparation, the samples were loaded within 10 min to the UHV system. The so-called "defective H-termination" (111-H def.) was achieved by storing the wet chemically prepared H-terminated sample for 4 weeks at $<10^{-9}$ mbar in UHV.

2.2. XPS

X-ray photoemission (XPS) measurements were obtained using a SPECS PHOIBOS 150 spectrometer in medium-area mode using a monochromatic Al Kα X-ray source (Focus 500 with XR50M (SPECS) with a photon flux of $\approx 1.8 \times 10^{11}$ photons/s at 300 W) with $h\nu = 1486.74$ eV normal to the surface. If not otherwise stated, survey and detail spectra were measured in fixed analyzer transmission mode with pass energy of 20 eV (step size of 0.5 eV) and 10 eV (step size of 0.05 eV), respectively. The spectrometer was calibrated by yielding the Fermi-level edge of Au, Ag, Cu to 0 eV binding energy (BE) as well as $BE(Au4f_{7/2}) = 83.98$ eV, $BE(Ag3d_{5/2}) = 368.26$ eV, and $BE(Cu2p_{3/2}) = 932.67$ eV with deviations $\leq$50 meV. Ultraviolet photoemission (UPS) measurements were conducted on the same spectrometer with pass energy of 5 eV (step size of 0.05 eV) using the helium lamp HIS 13 Mono (Focus GmbH) as monochromatic HeII source with $h\nu = 40.81$ eV normal to the surface if not specified otherwise. Cryomeasurements were conducted by cooling with liquid nitrogen leading to a substrate temperature of about −176 °C.

2.3. XAS

Near-edge X-ray absorption fine structure (NEXAFS) measurements were performed on the SoLiAS endstation at the undulator beamline UE56-2_PGM-2 at the BESSY II synchrotron. XAS were obtained in partial electron yield (PEY) using a SPECS PHOIBOS 150 spectrometer in constant-final-state mode. Si $L_{2,3}$ and the O K-edges were measured at kinetic energies of 93.9 and 474.9 eV, respectively, using step sizes of 0.1 eV.

3. Results and Discussion

In the following experiments, we mainly focus on the energetic position of the spectra in order to determine band bending and SPV depending of the applied surface preparation. In **Figure 1**, the survey spectra of p-Si surfaces after the different pretreatments are shown with detailed spectra of the Si 2*p* and O 1*s* emission. The related BE values of the Si $2p_{3/2}$ line for all considered samples are given in Table 1. Our XPS measurements show that in addition to emissions from Si, only O emissions appear on the sample. Furthermore, traces of carbon contamination are only found on air exposed as well as on the flash-annealed samples which we assign to adventitious carbon not affecting surface band bending. For that reason, we focus in the following discussion on surface states on pure silicon and oxidized surfaces.

The energetic position of the Si 2*p* line depends on the charge carrier concentration in the bulk as well as on the defect concentration at the silicon surface. The majority charge carrier concentration for each Si wafer was derived from Hall measurements given in **Table 2**.

From the measured majority charge carrier concentration, the bulk Fermi-level position E_F with respect to valence band E_{VB} and conduction band positions E_{CB} can be determined according to Equation (2) and (3) for p- and n-type semiconductors with respective acceptor concentration N_A and donor concentration N_D.

$$E_{VB} - E_F = k_B{\cdot}T{\cdot}\ln\left(\frac{N_A}{N_{VB}}\right) \quad (2)$$

$$E_F - E_{CB} = k_B{\cdot}T{\cdot}\ln\left(\frac{N_D}{N_{CB}}\right) \quad (3)$$

Both the valence and conduction band in Si are formed by sp^3-related bonding and antibonding σ and σ^* combinations. Due to missing bonding partners at the surface, dangling bonds form a characteristic surface state distribution N_{SS} inside the bandgap. Depending on the surface state distribution with respect to the bulk Fermi-level, charge transfer from the surface into the bulk occurs and induces band bending toward the surface.

By making use of the invariant energetic difference of the Si 2*p* core-level line to the valence band maximum (VBM) $\Delta E_{VS} = E_{Si2p_{3/2}} - E_{VBM}$, the Fermi-level position at the surface can be precisely determined by the position of the Si 2*p* line. In case of crystalline silicon, ΔE_{VS} is equal to 98.74 eV and is independent of doping and surface band bending.[22] With that, the Fermi-level position at single-crystalline Si surfaces can be derived by $E_{VBM} - E_F = E_{Si2p_{3/2}} - 98.74$ eV. In principle, these values can be determined by the HeII valence band edge (see Figure 3) as well. However, for comparing these values, a precise evaluation of the valence band onset, contributions of surface states, and modified source-induced photovoltages must be considered.

3.1. Intrinsic Dangling Bond States at Silicon Surfaces

Trivalent $Si_3 \equiv Si{\cdot}$ dangling bonds are known to form two corresponding states inside the bandgap of Si with one donor state (bonding state) at around 0.25 eV and one acceptor state

© 2023 The Authors. Solar RRL published by Wiley-VCH GmbH

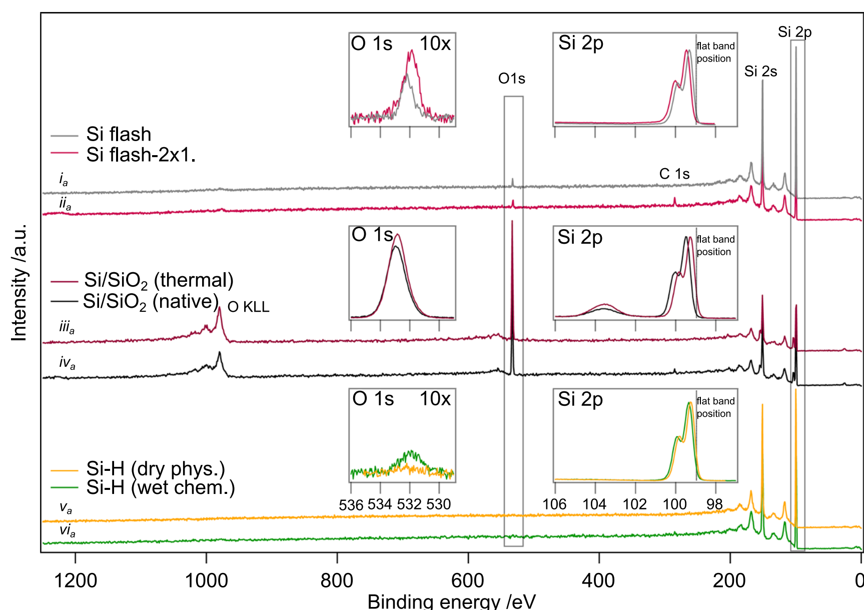

Figure 1. XP spectra of prepared flash-annealed (top), oxide-terminated (middle), and hydrogen-terminated p-Si surfaces with normalized Si 2p and O 1s detailed spectra.

Table 2. Fundamental properties of Si wafers used in this work with sheet conductivity, charge carrier concentration, and charge carrier mobility as derived from Hall measurements (in van der Pauw measurement geometry with a magnetic field B = 1.3 T).

Si wafer (orientation)	Dopant	Sheet conductivity in [S cm^{-1}]	Bulk charge carrier concentration in cm^{-3}	Mobility in cm^2 Vs^{-1}	Flat band E_F-E_{VB} in eV
p-Si (100)	Boron	0.15	3.2E15	290	0.22
p-Si (111)	Boron	0.11	2.5E15	270	0.22
p-Si (100)[a)]	Boron	0.67	3.8E16	111	0.16
n-Si (100)	Phosphorous	0.19	9.3E14	1270	0.86
n-Si (111)	Phosphorous	0.10	4.6E14	1330	0.84
n-Si (100)[a)]	Phosphorous	110	1.9E18	102	1.02

[a)]H_2-annealed H-terminated Si from TU Ilmenau.

(antibonding state) at about 0.85 eV above the VBM.[23,24] The amphoteric character of this dangling bond defect leads to a U-shape distribution around midgap with the charge neutrality level (CNL) of about 40 meV below midgap position.[25]

The detailed Si 2p spectra of flashed n- and p-doped Si(100) surfaces are depicted in **Figure 2**a, without any visible oxide species that should be located at higher binding energies in the range of BE = 103 eV. The peak maximum of the Si 2$p_{3/2}$ emission of the p-doped sample is located at BE = 99.34 eV, which correlates with a midgap Fermi-level position of 0.60 eV above the VBM. In contrast, the n-doped surface reveals a higher Fermi-level position shifted by further 0.2 eV toward higher binding energies. However, the reduction of the X-ray intensity by lowering the source power from 300 to 10 W leads to a downward shift of the Fermi-level of the n-doped sample nearly to the same position as observed for the p-doped sample. The correlation of X-ray intensity versus binding energy on the n-doped surface indicates a source-induced SPV, reducing the initial band bending at the n-doped surface. In contrast, the binding energy of the p-doped sample seems to be independent of the variation of the X-ray intensity, which is most probably related to the much lower majority charge carrier mobility for the p-doped sample (more than four times lower than for n-doped sample (Table 1). The identical energy position at low X-ray intensities for both, the n- and p-type sample, respectively indicates a strong surface Fermi-level pinning which is independent of the bulk doping N_{Dopant} concentration. Fermi-level pinning is expected for ionized surface state concentrations $N_{SS} > \sqrt{2\varepsilon\varepsilon_0 E_g N_{Dopant}}$ as this corresponds to the maximum charge stored in the semiconducting space–charge region with a bandgap of E_g. In our case, the pinned Fermi-level position coincides with the CNL of the Si dangling bond states, indicating $N_{SS} \gg 10^{11}$ cm^{-1} as most of the surface states remain uncharged close to the CNL (Figure 2b). It can be concluded that after flashing of the Si surface, the number of dangling bond states approaches the number of Si surface atoms.

The high amount of Si dangling bonds straight after flashing leads to a high surface reactivity of the surface as observed in the HeII spectra in **Figure 3**a, revealing a progressing, rapid hydroxylation of the surface even at a base pressure below 8×10^{-10} mbar. Two rising features at BE = 7 eV and BE = 12 eV which correspond to the 1π and 3σ antibonding and bonding orbitals of OH[26] appear after a short time and increase in intensity. For the flashed sample, gap states arise 0.2 eV below the Fermi-level, as shown in Figure 3b. It is yet not clear whether these gap states originate from dangling bonds as discussed before or from the π-interaction of Si dimers at the surface forming the 2 × 1 surface reconstruction.[27,28] These gap states vanish with the ongoing hydroxylation and consequently no surface

© 2023 The Authors. Solar RRL published by Wiley-VCH GmbH

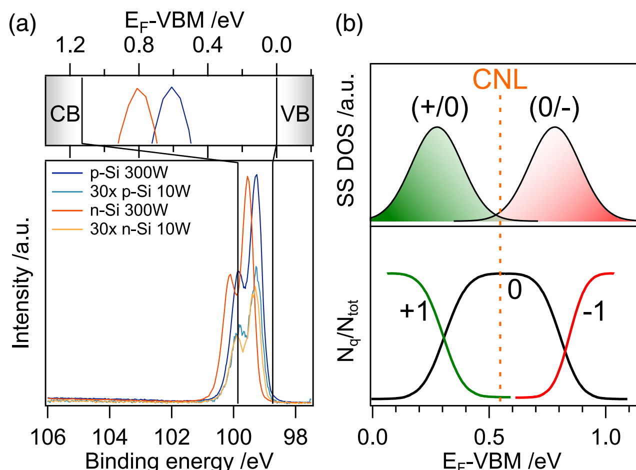

Figure 2. a) Si 2p spectra of flashed n- and p-doped Si(100) surfaces with different X-ray source intensities. Binding energy dependence on light intensity indicates SPV. Higher X-ray intensity with X-ray power of 300 W flattens initial surface band bending. Fermi-level positions are derived from BE(Si2$p_{3/2}$)-98.74 eV at 10 W X-ray power and seem to be independent of bulk doping. b) Schematic surface states' distribution of Si dangling bonds with charge occupation N_q/N_{tot} depending on surface Fermi-level position and marked CNL according to another study.[45]

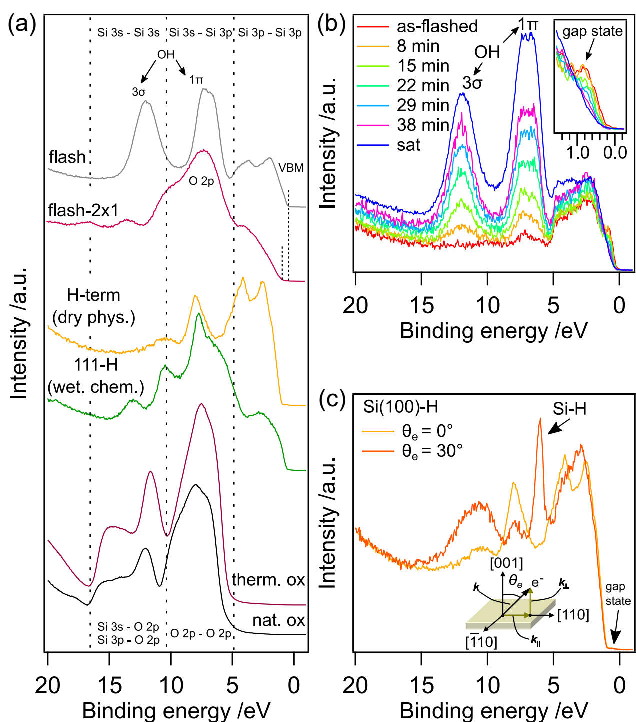

Figure 3. a) HeII spectra of prepared p-Si surfaces with depicted valence state regions (represented by the broken lines). b) Progressing hydroxylation of flashed Si(100) surface when stored at base pressures below 8×10^{-10} mbar. c) UHV H-terminated n-Si(100) surface at an emission angle θ_e 0° and 30° hydrogen feature at 6 eV.

reconstruction can be observed by LEED. However, the surface Fermi-level position seems to be unaffected by these gap states, which still indicates a high concentration of remaining dangling bond states. Only after subsequent annealing of the surface in UHV, a two-domain 2 × 1 LEED pattern with domains orientated perpendicular to each other indicates a stable Si dimer formation (Figure S1, Supporting Information). However, specific emissions appear in the He II spectra at BE = 7 and 11 eV which are related to the O 2p σ- and π-bonding states. Moreover, the XPS O 1s emission shows a chemical shift from the hydroxide species at BE = 532.2 eV to a more oxidic species at BE = 531.8 eV (Figure 1). As a result, the VBM shifts to higher binding energies in the same manner as the Si 2p line, indicating an upward Fermi-level shift to 0.7 eV above the VBM resulting from oxygen-induced donor states localized above midgap.

3.2. Oxygen-Related Dangling Bond Defects

The σ and π interactions of oxygen with silicon atoms are capable of passivating surface defects as bonding and antibonding states formed by Si sp^3 hybrid orbitals interacting with O sp hybrids, and O 2s and O 2p contributions appear below the band edges.[29] HeII spectra of oxidized silicon surfaces show broad O 2p emissions at around 7 eV (Figure 3a). In addition, the Si 3s-, Si 3p-, and O 2p-related states reveal a characteristic valence band feature at 12 eV and around 14 eV.[30] The sputter annealing procedure of the bare wafer leads to pronounced valence band features indicating a well-defined oxide layer which seems to be homogeneous and stoichiometric. In the Si 2p core-level region, broadened SiO_2-related contributions appear between 103.5 and 103.8 eV dependent on substrate doping with FWHM of about 1.5 eV (Figure 1). From the SiO_2 to Si ratio of the Si 2p region, an oxide layer thickness of around ≈8.1 Å with an O-to-Si ratio of about 2:1 (66 at% O and 33 at% Si) has been derived from Equation (1) for the untreated wafer. After sputter annealing, the thickness increased to ≈10.5 Å with no significant change in the oxide stoichiometry. Detailed oxide thickness and stoichiometry calculations can be found in Table S2 and S3, Supporting Information. For entropy reasons, even a fully oxidized Si surface possesses dangling bond defects. In this case, the surface state distribution in the bandgap strongly depends on the oxidation state of the defect centers induced by dangling bonds. These partially oxidized P_b centers can be assigned to either $Si_2O_1 \equiv Si\cdot$ or $Si_1O_2 \equiv Si\cdot$ structures, respectively. They are known to show only donor-like states within the Si bandgap at around 0.4 and 0.7 eV above the VBM, revealing a narrower distribution than the symmetrical midgap states.[31] The donor state of the $O_3 \equiv Si\cdot$ center is expected to be even above the CBM, thus related to a fixed positive oxide charge.[25] For the native oxide termination both, p- and n-type Si, respectively show donor-like surface defects. This results in an inversion layer at the surface of the p-Si as the Fermi-level is located 0.74 eV above the VBM which is slightly above midgap position. For the n-Si, an electron accumulation at the surface is observed as well since donor states shift the Fermi-level to 1.00 eV above the VBM which is located 0.13 eV above the flatband position in the bulk. Due to the temperature treatment, excess dangling bonds are consumed by the reaction with oxygen and to some extent by the reaction with silicon, leading to a more pronounced flatband-like situation than the initial native oxide termination does. The p-Si reduces the

© 2023 The Authors. Solar RRL published by Wiley-VCH GmbH

initial downward band bending by 0.13 to 0.29 eV. On n-Si, the Fermi-level equals the flatband position. In contrast to bare Si, the Fermi-level position for the oxide-terminated Si seems to be independent of the source intensity. The reason for the more pronounced flatband situation on n-Si/SiO_2 compared to p-Si/SiO_2 is attributed to the amphoteric interaction of the P_b acceptor states above midgap and partially oxidized P_b-centers acting as donors accordingly.

3.3. Dangling Bond Passivation by Hydrogen Termination

Saturating Si dangling bonds with atomic hydrogen is a well-known surface treatment to passivate the dangling bond states at Si surfaces. In this study, we compare wet chemical treatment according to another study[7] with dry physical treatment at elevated temperatures under 950 mbar H_2 ambient right away transferred to UHV according to Brückner et al.[18] It turns out that the H_2-prepared Si–H samples are extremely clean and that they show neither carbon nor oxygen contamination, respectively (Figure 1, yellow spectrum). However, it has to be mentioned that the H_2-based treatment in the MOCVD chamber leads to an unwanted contamination with arsenic coming from previous growth runs of III–Vs. Even though As is well known as a shallow donor in Si, no indications for any bonded As states could be observed with XPS or RAS methods (Figure S4, Supporting Information). By applying dedicated fitting routines, the Si 2p emission can be deconvoluted resulting in separated single Si 2p components with different 2p doublet structures suggesting different backbonding centers. We find a surface-related component with a chemical shift of about 0.25 eV to higher binding energies compared to the bulk-related $Si_3 - Si_3$ center (Figure S4, Supporting Information) that can be assigned to $Si_3 \equiv Si - H$.[32] In addition, RAS and LEED pattern (Figure S4 and S5, Supporting Information) reveal a 2×2 reconstructed surface indicating a monohydride surface phase with a prevalence of a 1×2 domain.[18,33]

24 h after preparation, the n-Si:H sample exhibits a binding energy position of the core level of $BE(Si2p_{3/2}) = 99.85$ eV and a Fermi-level position of 1.01 eV above the VBM. According to the higher doping concentration of the wafer, which was used for this sample, the measured value is only 30 meV below the calculated bulk position, indicating flatband situation at the surface. For p-Si:H, the Si 2p appears at $BE(Si2p_{3/2}) = 99.23$ eV which can be assigned to a Fermi-level located 0.49 eV above the VBM in contrast to the calculated bulk position of 0.16 eV. Nevertheless, source-induced SPV plays a role for both samples since reduced light intensity moves the Fermi-level 100 meV toward midgap in both cases, n- and p-type Si, respectively. In order to obtain these energy shifts in n-Si, the source intensity needed to be decreased from 300 to 1 W. In contrast to that, it was sufficient to decrease the source-intensity for the p-Si-H to 10 W showing again that the depleted n-Si layer is more susceptible against SPV than p-Si. The HeII line of the Si(100):H prepared samples shows two degenerated Si 3p features at around 2.5 and 4.1 eV (Figure 3c). At 8 eV, a strong Si 3s–3p peak arises whereas the broad feature at around 10.5 eV is of more 3s character. By reducing the photoelectron emission angle θ_e from 0° to 30° in azimuthal [110] direction shown in Figure 3c,[33] one can probe the surface Brillouin zone from the Γ to the J-point showing a very sharp peak at 6.0 eV which can be associated to Si–H surface bonding and is in good agreement with previous findings and tight binding calculations at the J-point.[34,35] Despite the well-defined surface with almost flatband condition, the HeII spectrum reveals a small amount of states showing up above the valence band edge up to the Fermi-level with a small peak structure, 290 meV above the VBM, which we attribute to the occupied Si dangling bond state. 48 h after preparation, the Si 2p line of the n-doped Si shifts about 200 meV down to $BE(Si2p) = 99.63$ eV which seems to be source intensity independent and thus indicates a strong Fermi-level pinning 0.89 eV above the VBM due to partially H desorption increasing the amount of Si dangling bond states in UHV.

During the wet chemical H-termination treatment, the native oxygen is etched and remaining dangling Si bonds are terminated in NH_4F solution with atomic hydrogen. The H-terminated samples were loaded within 10 min after preparation into the XPS analysis chamber. The prepared H-terminated surfaces reveal low oxygen contents of less than 1.5 at% with XPS. However, the HeII spectra reveal clear indications of surface oxidation as shown by a broad O 2p feature at around 5–10 eV (Figure 3a). At the same time, the VBM from Si 3p states and the Si 3s–3p feature at 8 eV are clearly visible, while the oxidized contributions appear as two features at 11 and 13 eV. Both preparations led to 1×1 reconstructed surfaces, indicating a fully hydrided surface with no dimer formation on both (111) and (100) surfaces (Figure S6, Supporting Information).[8] Energetically, H-terminated n-Si(100) and (111) show a Fermi-level position very close to the conduction band $BE(Si2p_{n-111}) = 99.88$ eV and $BE(Si2p_{n-100}) = 99.94$ eV indicating an accumulation surface layer due to oxygen-related donor states similar to the oxygen-terminated surfaces as discussed before. The H-terminated p-doped surfaces show for both orientations a midgap Fermi-level position at $BE(Si2p) = 99.35$ eV. In case of p-Si, donors and acceptors of partially oxidized and nonoxidized P_b centers pin the Fermi-level 0.6 eV above the VBM. On n-Si, the acceptor states are fully occupied due to the higher bulk Fermi-level. In combination with the oxygen-related donor states, this results in an electron accumulation at the surface. This is in good agreement with Schlaf et al. who found a strong donor level pinning the Fermi-level at 0.2 eV below the CBM for HF-etched p- and n-Si surfaces.[11] Storing the p-Si(111):H sample for 4 weeks at $<10^{-9}$ mbar led to further surface oxidation, and a Fermi-level shift of 50 meV toward the conduction band indicating further oxygen-induced electron accumulation.

To investigate nonoccupied acceptor states inside the Si bandgap, we conducted X-ray absorption spectroscopy (NEXAFS) of wet chemically H-terminated Si surfaces. In Figure S7, Supporting Information, the Si $L_{2,3}$ and the O K-edges are shown. In this case, the n-(111) surface shows almost no absorption in the O–K edge region, indicating the lowest amount of surface oxidation. At the same time, the n-111 Si samples reveals the most prominent pre-edge feature 0.4 eV below the main Si absorption L-edge starting at $h\nu = 99.75$ eV, which we assign to the Si dangling bond acceptor states. The same state is also observed on (100) surfaces. The observed acceptor state on the wet chemical (111) and (100) surfaces coincides with the pinning level of the 48 h-altered

© 2023 The Authors. Solar RRL published by Wiley-VCH GmbH

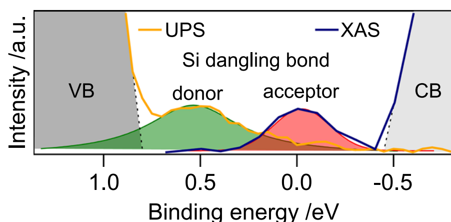

Figure 4. In-gap states of Si dangling bonds at H-terminated Si surfaces. UPS and XAS reveal occupied and unoccupied dangling bond states, respectively. UPS is taken from a UHV-prepared n-Si(100)-H (as extracted from Figure 3c) and XAS from a wet chemically prepared n-Si(111)-H surface (as extracted from Figure S7, Supporting Information). VB cutoff and XA onset were normalized to midgap states and separated by the optical bandgap of around 1.2 eV.

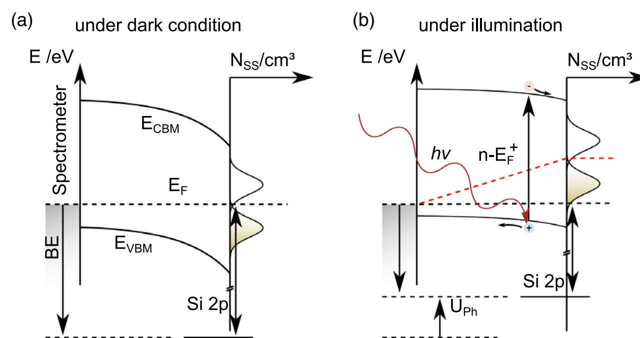

Figure 5. Scheme of a depleted p-Si surface with dangling bond states a) in the dark and b) under illumination where SPV lead to more flatband conditions, due to a higher concentration of electrons in the space–charge region indicated by their quasi-Fermi-level n-E_F^+.

UHV H-terminated (100) surface, indicating that Si dangling bonds are the dominating defects on both surfaces. Samples, which do not show this prominent pre-edge feature in the XAS, reveal significant amounts of oxygen confirming that the acceptor states of the oxidized P_b centers are located far above the CBM leading to only donor states within the Si bandgap.[25] **Figure 4** represents the whole surface state distribution of nonoxidized Si dangling bond centers within the bandgap according to our measurement results.

3.4. Source-Induced Photovoltages at Cryogenic Temperatures

Band bending due to surface states leads to a charge separation of excess charge carriers while illumination and with that induces SPV. The measurement of SPVs depending on light intensity is thus an easy experimental tool to characterize the quality of surface preparation as the surface recombination will strongly be affected by the number of surface states.[36] We showed that even under fully dark conditions of external light sources, the X-ray source itself can induce SPV (Figure 2a). In addition to the absorption properties, source-induced SPVs at a depleted space charge region due to surface states mainly depend on two semiconductor properties. One is the charge carrier diffusion length of majority as well as the minority charge carriers which need to be separated from the surface into the bulk and vice versa. Another factor for the extent of SPV is the lifetime of the minority charge carriers in the bulk compared to the surface. For high mobilities and bulk carrier lifetimes, most of the nonequilibrium charge carriers will contribute to the separation of the minority carriers. Usually, the mobility of charge carriers at surfaces is considerably lower than in the bulk since Coulomb scattering occurs at charge carriers trapped at surface states.[37] The effective lifetime of charge carriers at the surface is mainly limited by Shockley–Read–Hall recombination involving surface states.

We used cryo-XPS measurements for probing the space–charge region at the prepared silicon surfaces. At liquid nitrogen temperature, the Fermi-level position moves closer to the conduction band due to a "freeze-out" of doping levels and the bandgap increases by about 40 meV which leads finally to a bulk Fermi-level of $E_{VB} - E_F(-176\,°C) = 0.08\,eV$ and $E_{CBM} - E_F(-176\,°C) = 0.09\,eV$ for the p-Si and n-Si wafers, respectively. Furthermore, we observe a reduction of the surface band bending, indicating a higher SPV at liquid nitrogen temperature, which results in approaching flatband condition.[38–40]

Figure 5 depicts the surface band bending of p-Si surface in the dark and illuminated conditions. The observed ionized donor states in Si surfaces will lead to a positive charged surface. If we assume that under illumination the total surface charge will not change, source-induced excess charge carriers will screen the fixed surface charge and thereby reduce the initial surface band bending.[41] As a result, source-induced SPVs always lead to a decrease of apparent band bending. This effect can be pronounced by cooling the sample to liquid nitrogen.[38,39] As the thermally induced transitions of holes as majority carriers are exponentially reduced with temperature, the recombination of excess charge carriers with intrinsic counter charges is suppressed which also leads to strong temperature dependence of the reverse saturation current density of the rectifying space–charge region.[42] This effect can be enhanced using bias light in addition, which may even lead to nearly flatband conditions in the respective measurements.[11]

The Fermi-level positions within the Si bandgap for all p- (bottom row) and n-Si surfaces (top row) as evaluated from the Si $2p_{3/2}$ position according to Table 1 are depicted in **Figure 6** in comparison to the expected flatband potential from Table 2. The bars represent the total surface band bending by the difference between the measured surface Fermi-level position and the calculated bulk Fermi-level position (dashed lines) at room (green) and liquid nitrogen (red) temperature. The shift of bulk Fermi-level position after cooling is related to a freeze-out of dopants. The bandgap of the Si–H (dry) sample was reduced due to the high doping concentration of the n-type wafer narrowing the bandgap.[43] The size reduction of bars from room (green) to iquid nitrogen temperature (red) can be considered as source-induced SPV at low temperature. The extent of SPV gives conclusions about the total amount of surface defects and to what extent they can act as recombination centers for excess charge carriers. At room temperature, all p-Si samples show a depletion region due to the previous discussed donor states inside the Si bandgap at the surface. In contrast to that, only oxygen-free samples (flashed and dry-H-terminated Si) reveal a slight electron depletion in n-Si surfaces, due to unoccupied acceptor levels below the bulk Fermi-level. All other n-Si surfaces show either flatband (therm. Ox) or electron accumulation at the surface, due to oxygen-related donors close to the CBM. From the above

© 2023 The Authors. Solar RRL published by Wiley-VCH GmbH

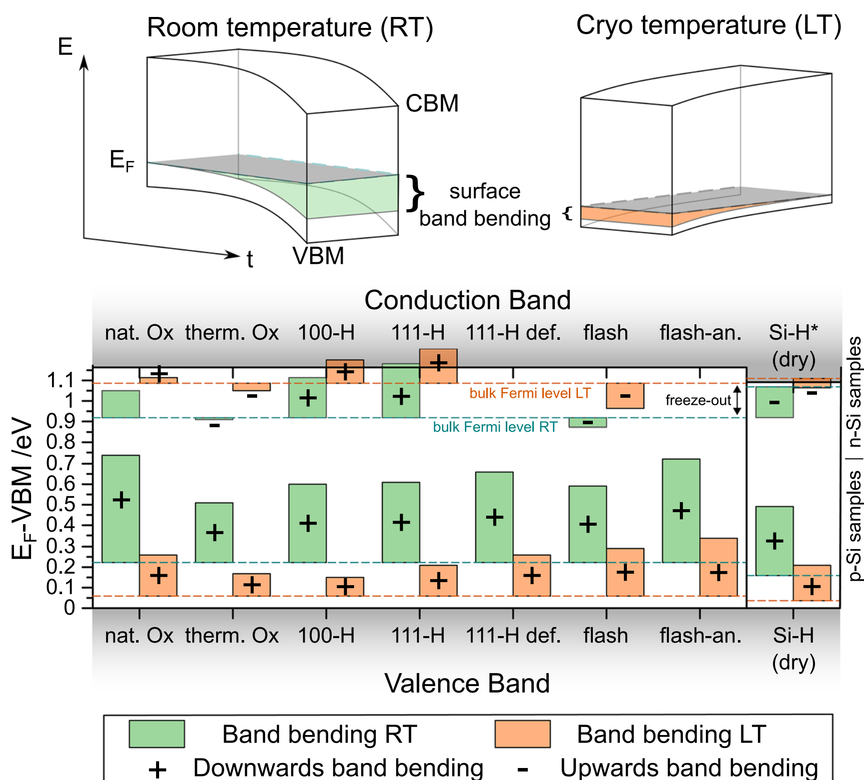

Figure 6. 2D projection of SCR inside the Si bandgap of all samples due to surface band bending at room temperature (green) and liquid nitrogen temperature (red). Bottom and top row represent p-Si and n-Si samples, respectively. Bar edges indicate Fermi-level to VBM energy difference in the bulk and at the surface. Reduction of band bending at liquid nitrogen temperature indicates a source-induced SPV. *Bandgap narrowing and different bulk Fermi-level positions due to higher doping concentration of used wafer for sample Si-H dry.

shown set of samples, we draw the following conclusions: 1) oxygen-free surfaces show lower source-induced SPV at low temperature indicating that the recombination activity of the Si dangling bonds gets reduced by the oxidation of P_b centers, what is in good agreement with Flietner[31] who attributed the main recombination activity to the nonoxidized dangling bond states as the amphoteric character of this defect enhances the Shockley–Read–Hall process when the splitting of quasi-Fermi-level at midgap ionizes donors and acceptors simultaneously. 2) All p-Si surfaces show larger band bending than equivalent n-Si surfaces as already observed elsewhere.[11] We attribute this behavior to the following observations: clean n-Si surfaces are more susceptible against SPV even at room temperature as discussed above, what makes the evaluation of total band bending by PES almost impossible. Furthermore, the oxidation of dangling bond centers shift acceptor levels above the conduction band and prevent upward band bending. 3) The sputter-annealed sample (therm. Ox) shows for n- and p-type the lowest band bending at room and low temperature, indicating that the total amount of surface states is the lowest in comparison to all other samples.

4. Conclusion

We investigated the role of Fermi-level pinning due to Si dangling bonds on different Si (100) and (111) surfaces. Our findings on flashed Si surfaces confirm the amphoteric U-shape distribution of Si dangling bond centers. Both p- and n-type Si show midgap Fermi-level pinning which coincides with the CNL of the Si dangling bond center. Furthermore, on completely oxygen-free surfaces, we found an occupied in-gap state 0.29 eV above VBM and an unoccupied in-gap state 0.40 eV below the CBM, which coincide with these dangling bond states. According to our results, oxygen-contaminated surfaces show electron accumulation, since the unoccupied in-gap states vanish and lead to only donor-like states remaining inside the bandgap. We attribute these oxygen-related donors to partially oxidized Si dangling bond centers. For that reason, none of our prepared p-surfaces reveal flatband conditions while n-surfaces show lower surface band bending. However, from that we conclude that flatband is not a sufficient condition to identify defect-free surfaces as only ionized surface states lead to surface band bending. Moreover, Fermi-level pinning requires the amphoteric character of a defect center. For high defect concentrations, the pinning level will correspond to the CNL of the defect, provided that there are electronic states at this energy. In this case, the electronic distribution of the defect plays a minor role for the pinning itself. For lower defect concentrations, the amphoteric character is provided by the defect itself when neutral and ionized states coexist and lead to a half-filled defect band. As a result, the same surface defect but different concentrations lead to different pinning positions inside the bandgap. Furthermore,

© 2023 The Authors. Solar RRL published by Wiley-VCH GmbH

our cryo-XPS measurements indicated that donor-like oxidized P_b centers reveal lower recombination activities than the amphoteric nonoxidized dangling bond centers. According to our results, none of the investigated surfaces could be considered as defect free. However, a sputter-annealed oxide layer led to the best surface passivation for photoelectrochemical applications; as for p- and n-Si, the lowest surface band bending is observed at room temperature but also liquid nitrogen temperature, indicating the lowest recombination activity of excess charge carriers. Therefore, we can confirm based on our surface studies that controlled surface oxidation of Si, leading to a mostly defect-free Si/SiO_2 interface, will provide the most efficient surface passivation. However, even on the outermost SiO_2 surface layer, surface states may be induced when forming the contact to additional contact layers (e.g., to electrolyte molecules), which may again induce unfavorable space–charge layers.[10,44] Furthermore, the oxide layer may act as a tunnel barrier at the electrochemical interface and thus limit the charge transfer properties of the interface and with that the efficiency of the overall device. In conclusion, all of these aspects have to be taken into account when preparing proper passivation layers for photovoltaics and photoelectrochemical cells.

Supporting Information

Supporting Information is available from the Wiley Online Library or from the author.

Acknowledgements

The authors acknowledge the financial support of this work by the DFG (PAK981: project no. 424924805) and BMBF (GEP-HE: Project No. 13XP5023A). The authors thank the Helmholtz-Zentrum Berlin (HZB) for allocation and synchrotron beamtime at BESSY II. SoLiAS endstation is funded by BMBF (project no. 05 KSIRD1/0). In addition, the authors thank Prof. Andreas Klein and Kim Alexander Creutz for providing the Hall measurement setup.

Open Access funding enabled and organized by Projekt DEAL.

Conflict of Interest

The authors declare no conflict of interest.

Data Availability Statement

The data that support the findings of this study are available from the corresponding author upon reasonable request.

Keywords

band bending, cryophotoemission spectroscopy, Fermi-level pinning, H termination, Si surface states, surface photovoltages

Received: November 28, 2022
Published online: February 17, 2023

[1] W. H. Cheng, M. H. Richter, M. M. May, J. Ohlmann, D. Lackner, F. Dimroth, T. Hannappel, H. A. Atwater, H. J. Lewerenz, *ACS Energy Lett.* **2018**, *3*, 1795.
[2] F. Urbain, V. Smirnov, J. P. Becker, A. Lambertz, F. Yang, J. Ziegler, B. Kaiser, W. Jaegermann, U. Rau, F. Finger, *Energy Environ. Sci.* **2016**, *9*, 145.
[3] T. Mayer, K. Schwanitz, B. Kaiser, A. Hajduk, M. V. Lebedev, W. Jaegermann, *J. Electron. Spectrosc. Relat. Phenom.* **2017**, *221*, 116.
[4] J. P. Becker, F. Urbain, V. Smirnov, U. Rau, J. Ziegler, B. Kaiser, W. Jaegermann, F. Finger, *Phys. Status Solidi* **2016**, *213*, 1738.
[5] B. M. Kayes, H. A. Atwater, N. S. Lewis, *J. Appl. Phys.* **2005**, *97*, 114302.
[6] M. Grundner, H. Jacob, *Appl. Phys. A: Solids Surf.* **1986**, *39*, 73.
[7] H. Angermann, W. Henrion, M. Rebien, J.-T. Zettler, A. Röseler, *Surf. Sci.* **1997**, *388*, 15.
[8] J. J. Boland, *Phys. Rev. Lett.* **1990**, *65*, 3325.
[9] M. M. May, H.-J. Lewerenz, D. Lackner, F. Dimroth, T. Hannappel, *Nat. Commun.* **2015**, *6*, 8286.
[10] S. Tengeler, M. Fingerle, W. Calvet, C. Steinert, B. Kaiser, T. Mayer, W. Jaegermann, *J. Electrochem. Soc.* **2018**, *165*, H3122.
[11] R. Schlaf, R. Hinogami, M. Fujitani, S. Yae, Y. Nakato, *J. Vac. Sci. Technol., A* **1999**, *17*, 164.
[12] E. H. Poindexter, P. J. Caplan, *Prog. Surf. Sci.* **1983**, *14*, 201.
[13] M. A. Jupina, P. M. Lenahan, *IEEE Trans. Nucl. Sci.* **1989**, *36*, 1800.
[14] S. Tanuma, C. J. Powell, D. R. Penn, *Surf. Interface Anal.* **1991**, *17*, 927.
[15] M. P. Seah, S. J. Spencer, *Surf. Interface Anal.* **2002**, *33*, 640.
[16] J. H. Scofield, *J. Electron. Spectrosc. Relat. Phenom.* **1976**, *8*, 129.
[17] H. Döscher, O. Supplie, S. Brückner, T. Hannappel, A. Beyer, J. Ohlmann, K. Volz, *J. Cryst. Growth* **2011**, *315*, 16.
[18] S. Brückner, O. Supplie, A. Dobrich, P. Kleinschmidt, T. Hannappel, *Phys. Status Solidi* **2018**, *255*, 1700493.
[19] S. Brückner, H. Döscher, P. Kleinschmidt, O. Supplie, A. Dobrich, T. Hannappel, *Phys. Rev. B* **2012**, *86*, 195310.
[20] D. E. Aspnes, A. A. Studna, *Phys. Rev. Lett.* **1985**, *54*, 1956.
[21] T. Hannappel, S. Visbeck, L. Töben, F. Willig, *Rev. Sci. Instrum.* **2004**, *75*, 1297.
[22] F. J. Himpsel, G. Hollinger, R. A. Pollak, *Phys. Rev. B* **1983**, *28*, 7014.
[23] E. H. Poindexter, G. J. Gerardi, M. E. Rueckel, P. J. Caplan, N. M. Johnson, D. K. Biegelsen, *J. Appl. Phys.* **1984**, *56*, 2844.
[24] M. J. Uren, J. H. Stathis, E. Cartier, *J. Appl. Phys.* **1996**, *80*, 3915.
[25] W. Füssel, M. Schmidt, H. Angermann, G. Mende, H. Flietner, *Nucl. Instrum. Methods Phys. Res., Sect. A* **1996**, *377*, 177.
[26] D. Schmeisser, F. J. Himpsel, G. Hollinger, *Phys. Rev. B* **1983**, *27*, 7813.
[27] X.-Y. Ren, H.-J. Kim, C.-Y. Niu, Y. Jia, J.-H. Cho, *Sci. Rep.* **2016**, *6*, 27868.
[28] F. J. Himpsel, D. E. Eastman, *J. Vac. Sci. Technol.* **1979**, *16*, 1297.
[29] G. Hollinger, S. J. Sferco, M. Lannoo, *Phys. Rev. B* **1988**, *37*, 7149.
[30] J. L. Alay, M. Hirose, *J. Appl. Phys.* **1997**, *81*, 1606.
[31] H. Flietner, *Mater. Sci. Forum* **1995**, *185–188*, 73.
[32] H. J. Lewerenz, M. Aggour, C. Murrell, M. Kanis, H. Jungblut, J. Jakubowicz, P. A. Cox, S. A. Campbell, P. Hoffmann, D. Schmeißer, *J. Electrochem. Soc.* **2003**, *150*, E185.
[33] R. I. G. Uhrberg, G. V. Hansson, J. M. Nicholls, S. A. Flodström, *Phys. Rev. B* **1981**, *24*, 4684.
[34] K. Hricovini, R. Günther, P. Thiry, A. Taleb-Ibrahimi, G. Indlekofer, J. E. Bonnet, P. Dumas, Y. Petroff, X. Blase, X. Zhu, S. G. Louie, *Phys. Rev. Lett.* **1993**, *70*, 1992.
[35] K. C. Pandey, *Phys. Rev. B* **1976**, *14*, 1557.
[36] R. Chen, F. Fan, T. Dittrich, C. Li, *Chem. Soc. Rev.* **2018**, *47*, 8238.
[37] E. Arnold, G. Abowitz, *Appl. Phys. Lett.* **1966**, *9*, 344.

© 2023 The Authors. Solar RRL published by Wiley-VCH GmbH

[38] M. Alonso, R. Cimino, K. Horn, *Phys. Rev. Lett.* **1990**, *64*, 1947.
[39] A. Klein, Y. Tomm, R. Schlaf, C. Pettenkofer, W. Jaegermann, M. Lux-Steiner, E. Bucher, *Sol. Energy Mater. Sol. Cells* **1998**, *51*, 181.
[40] D. C. Moritz, I. A. Ruiz Alvarado, M. A. Zare Pour, A. Paszuk, T. Frieß, E. Runge, J. P. Hofmann, T. Hannappel, W. G. Schmidt, W. Jaegermann, *ACS Appl. Mater. Interfaces* **2022**, *14*, 47255.
[41] L. Kronik, Y. Shapira, *Surf. Sci. Rep.* **1999**, *37*, 24.
[42] A. Klein, T. Mayer, A. Thissen, W. Jaegermann, in *Methods in Physical Chemistry*, Wiley, Weinheim, Germany **2012**, pp. 477–512.
[43] R. J. Van Overstraeten, R. P. Mertens, *Solid State Electron.* **1987**, *30*, 1077.
[44] C. Steinert, S. Tengeler, B. Kaiser, W. Jaegermann, *J. Electrochem. Soc.* **2019**, *166*, H3208.
[45] P. Broqvist, A. Alkauskas, A. Pasquarello, *Phys. Rev. B* **2008**, *78*, 075203.

© 2023 The Authors. Solar RRL published by Wiley-VCH GmbH